

Implications of Compressed Supersymmetry for Collider and Dark Matter Searches

Howard Baer^a, Andrew Box^b, Eun-Kyung Park^a, and Xerxes Tata^b

^a*Department of Physics, Florida State University Tallahassee, FL 32306, USA*

^b*Department of Physics and Astronomy, University of Hawaii, Honolulu, HI 96822, USA*

E-mail: baer@hep.fsu.edu,abox@phys.hawaii.edu,
epark@hep.fsu.edu,tata@phys.hawaii.edu

ABSTRACT: Martin has proposed a scenario dubbed “compressed supersymmetry” (SUSY) where the MSSM is the effective field theory between energy scales M_{weak} and M_{GUT} , but with the GUT scale $SU(3)$ gaugino mass $M_3 \ll M_1$ or M_2 . As a result, squark and gluino masses are suppressed relative to slepton, chargino and neutralino masses, leading to a compressed sparticle mass spectrum, and where the dark matter relic density in the early universe may be dominantly governed by neutralino annihilation into $t\bar{t}$ pairs via exchange of a light top squark. We explore the dark matter and collider signals expected from compressed SUSY for two distinct model lines with differing assumptions about GUT scale gaugino mass parameters. For dark matter signals, the compressed squark spectrum leads to an enhancement in direct detection rates compared to models with unified gaugino masses. Meanwhile, neutralino halo annihilation rates to gamma rays and anti-matter are also enhanced relative to related scenarios with unified gaugino masses but, depending on the halo dark matter distribution, may yet be below the sensitivity of indirect searches underway. In the case of collider signals, we compare the rates for the potentially dominant decay modes of the \tilde{t}_1 which may be expected to be produced in cascade decay chains at the LHC: $\tilde{t}_1 \rightarrow c\tilde{Z}_1$ and $\tilde{t}_1 \rightarrow bW\tilde{Z}_1$. We examine the extent to which multilepton signal rates are reduced when the two-body decay mode dominates. For the model lines that we examine here, the multi-lepton signals, though reduced, still remain observable at the LHC.

KEYWORDS: Supersymmetry Phenomenology, Supersymmetric Standard Model, Dark Matter.

1. Introduction

Models of particle physics with weak scale softly broken supersymmetry are well-motivated by both theory and experiment. On the theory side, they stabilize the scalar sector that plays an essential role in the spontaneous breaking of electroweak symmetry, allowing a sensible extrapolation of particle interactions over many orders of magnitude in energy. On the experiment side, supersymmetric models naturally accommodate, *i*) gauge coupling unification, *ii*) a mechanism for electroweak symmetry breaking due to a large top quark mass, *iii*) a light Higgs scalar and decoupled superpartners in accord with precision electroweak measurements and *iv*) a neutral weakly interacting particle that can, as a thermal Big Bang relic, account for the observed cold dark matter (CDM) in the Universe.

In spite of the accolades, supersymmetric theories suffer from new problems not present in the Standard Model (SM). There are the big issues such as the flavor and the CP problems, as well as the fact that baryon and lepton numbers can potentially be violated at large rates. We have nothing new to say about these, and will evade these in the usual ways. A much less serious objection is the “supersymmetric little hierarchy problem” which simply states that the value of the parameter $-m_{H_u}^2$ (renormalized at the TeV scale) can be $\sim M_Z^2$ only if there are cancellations at the percent level, once experimental constraints on sparticle and MSSM Higgs scalar masses are incorporated. Another potential problem is that in many supersymmetric models, the lightest SUSY particle, usually the lightest neutralino, is bino-like, with a typical *thermal* relic density considerably larger than the measured CDM density $\Omega_{CDM} h^2 \sim 0.1$ [1] for sparticle masses larger than ~ 100 GeV.

Recently, Martin has observed that the latter two issues are ameliorated in a scenario [2] that he calls “compressed supersymmetry”. Within this framework, it is assumed that the MSSM is the effective field theory between M_{weak} and M_{GUT} . As in the mSUGRA model, universal scalar mass parameters are adopted at $Q = M_{\text{GUT}}$ but non-universal gaugino mass parameters are allowed. Specifically, Martin notes that if $3M_3(\text{GUT}) \sim M_2(\text{GUT}) \sim M_1(\text{GUT})$, the fine-tuning required to obtain small values of $|m_{H_u}^2|$ is considerably reduced. The low value of M_3 results in a SUSY spectrum where physical squark and gluino masses are closer in mass to uncolored sparticles than in models such as mSUGRA with unified gaugino masses, where one expects $m_{\tilde{q}} \sim m_{\tilde{g}} \gg m_{\tilde{W}_1}$. Thus the SUSY spectrum is “compressed” relative to models with gaugino mass unification.

Of particular interest to us are solutions with a compressed spectrum where the top squark \tilde{t}_1 is particularly light. In this case, if the neutralino annihilation channel $\tilde{Z}_1 \tilde{Z}_1 \rightarrow t\bar{t}$ is kinematically accessible in the early Universe, its reaction rate suffers no propagator suppression because of the light t - and u - channel stop exchange, and can lead to a neutralino relic abundance in accord with WMAP, even though the neutralino remains largely bino-like. In addition, as noted above, the low third generation squark masses feed into the evolution of the soft SUSY breaking Higgs mass $m_{H_u}^2$, causing it to evolve to much smaller (in magnitude) negative values than in the case of unified gaugino masses. Since $-m_{H_u}^2(\text{weak}) \sim \mu^2$ the little hierarchy problem is less severe than in models with unified gaugino masses.

Martin has shown that the compressed SUSY scenario is valid provided that

$$m_t < m_{\tilde{Z}_1} \lesssim m_t + 100 \text{ GeV}, \quad (1.1)$$

$$m_{\tilde{Z}_1} + 25 \text{ GeV} \lesssim m_{\tilde{t}_1} \lesssim m_{\tilde{Z}_1} + 100 \text{ GeV}, \quad (1.2)$$

where the lower limits above are imposed so that annihilation of neutralinos into top pairs is allowed at rest, and to reduce the impact of \tilde{t}_1 - \tilde{Z}_1 co-annihilation, while the upper limits should be viewed as soft. He displays an explicit case where the GUT scale gaugino masses are related according to

$$1.5M_1 = M_2 = 3M_3, \quad (1.3)$$

which can occur in models where the SUSY breaking F -term that seeds SUSY breaking gaugino masses transforms as a linear combination of a singlet and an adjoint field of the unifying $SU(5)$ group. The trilinear soft SUSY breaking term A_0 is set either to $-M_1$ or $-0.75M_1$. Since the $\tilde{t}_1 - \tilde{Z}_1$ mass gap is small in compressed SUSY, Martin recognized that two cases emerge which are relevant to LHC searches: one is characterized by when $\tilde{t}_1 \rightarrow c\tilde{Z}_1$ is the dominant top squark decay channel, while the other has a large enough mass gap that $\tilde{t}_1 \rightarrow bW\tilde{Z}_1$ can compete, and perhaps dominate, the two-body decay.

In fact, this whole scenario appears closely related to scenarios first pointed out by Belanger *et al.*[3] and independently by Mambrini and Nezri[4] and subsequently examined in detail in Ref. [5], where a reduced GUT scale gaugino mass M_3 leads to a small μ parameter, and ultimately to a mixed higgsino-bino \tilde{Z}_1 which can annihilate efficiently into vector boson pairs, ameliorating the SUSY little hierarchy problem, while in accord with the measured abundance of cold dark matter in the Universe. While the analyses of [3, 4] and [5] take low M_3 in an *ad hoc* fashion, the required gaugino mass pattern can also be obtained by allowing the SUSY breaking F -term to transform as appropriate linear combinations of fields contained in the symmetric product of two adjoints of the unifying gauge group[6]. We note here that a top-down scenario that naturally leads to low M_3 , low $|\mu|$ and light top squarks occurs in so-called mixed moduli-anomaly mediated SUSY breaking models, also referred to as mirage unification models, wherein moduli contributions give universal gaugino mass terms, but comparable gaugino mass splittings from anomaly-mediation reduce the value of M_3 , owing to the negative $SU(3)$ beta function[7]¹.

In this paper, we explore the phenomenological implications of compressed SUSY. We divide our discussion into two different model lines. In Case A (examined in Sec. 2), we adopt a model line from Ref. [5] which is continuously connected to mSUGRA via variation of the gaugino mass M_3 , but with a non-zero A_0 parameter. By dialing M_3 to smaller values, the top squark mass is decreased, and the relic density is ultimately dominated by annihilation to $t\bar{t}$ via light \tilde{t}_1 exchange. The neutralino, however, remains essentially bino-like.² The enhanced neutralino annihilation rate in turn implies an enhanced DM annihilation rate in the galactic halo[9], and we show that indirect DM search rates are

¹For a further model with compressed spectra, see Bae *et al.*, Ref. [8].

²If M_3 is reduced farther, the neutralino develops a significant higgsino component and leads to mixed higgsino dark matter as already mentioned, unless of course, this range of M_3 is forbidden because \tilde{t}_1 becomes the LSP.

thus enhanced relative to mSUGRA. In addition, the low μ value and low $m_{\tilde{q}}$ values typical of compressed SUSY result in enhanced rates for direct DM detection, and detection via muon telescopes. For this case, when the measured abundance of CDM is achieved, we arrive at a small mass gap solution where $\tilde{g} \rightarrow t\tilde{t}_1$ dominantly, followed by $\tilde{t}_1 \rightarrow c\tilde{Z}_1$. In addition, the dominant decays $\tilde{W}_1 \rightarrow b\tilde{t}_1$ and $\tilde{Z}_2 \rightarrow \tilde{Z}_1 h$ suggest that compressed SUSY LHC signatures are expected to be *lepton poor*, although robust rates for multi-jet + E_T^{miss} signals remain. We note, however, that $\tilde{Z}_2 \rightarrow Z\tilde{Z}_1$ has a branching fraction of a few percent. This, combined with the enormous rate for the production of sub-TeV scale gluinos (in the dark-matter-allowed regions) makes the multi-lepton signal observable in the cases we examined.

In Case B (examined in Sec. 3), we consider a model line from Martin[2] with $1.5M_1 = M_2 = 3M_3$. In this case as well, DM direct and indirect detection rates are larger than for the case of unified gaugino masses (with large $|\mu|$), and may possibly be detectable via ton size noble element detectors, or perhaps via anti-particle and gamma ray searches if the (currently undetermined) halo dark matter distribution turns out to be suitably clumpy, even though \tilde{Z}_1 remains dominantly bino-like. Since the mass gap $m_{\tilde{t}_1} - m_{\tilde{Z}_1}$ can be greater than $m_b + M_W$, we implement the 3-body decay $\tilde{t}_1 \rightarrow bW\tilde{Z}_1$ into Isajet 7.76 (which we use for spectra and event generation). We find regions with a large branching fraction for $\tilde{t}_1 \rightarrow bW\tilde{Z}_1$ decays, so that when this mode dominates, leptonic signals from gluino and squark cascade decays occur at observable levels.

2. Case A: Low M_3 scenario with continuous connection to mSUGRA

In this section, we examine a model line based on mSUGRA, but with $M_3(\text{GUT})$ as an independent parameter, with parameter space

$$m_0, m_{1/2}, M_3, A_0, \tan\beta, \text{sign}(\mu), \quad (2.1)$$

where we take the GUT scale values³ $M_1 = M_2 \equiv m_{1/2}$ and adopt $m_t = 175$ GeV to conform with Martin[2]. The phenomenology of this scenario has been investigated in depth in Ref. [5] for $A_0 = 0$, where a low enough value of $M_3 \ll m_{1/2}$ leads to a small μ parameter, and hence the correct dark matter relic abundance via mixed higgsino DM. In the case studied here, we adopt a value of $A_0 = -1.5m_{1/2}$, which helps reduce $m_{\tilde{t}_1}$ compared with a choice of $A_0 = 0$, so that we can obtain dominant $\tilde{Z}_1\tilde{Z}_1$ annihilation into $t\bar{t}$ via a light \tilde{t}_1 exchange. Of course, if $m_{\tilde{t}_1} - m_{\tilde{Z}_1}$ becomes small enough, $\tilde{t}_1\tilde{Z}_1$ co-annihilation will also be important. Since for a bino-like LSP $m_{\tilde{Z}_1} \sim 0.4m_{1/2}$, we will need $m_{1/2} \gtrsim 450$ GeV so that $m_{\tilde{Z}_1} > m_t$. Thus, we adopt $m_{1/2} = 500$ GeV, and take $m_0 = 340$ GeV, $\tan\beta = 10$ and $\mu > 0$ in accord with Martin[2].

The mass spectrum – generated using Isajet 7.76[10] – is shown versus M_3 in Fig. 1a). In our illustration, $M_3 = 500$ GeV corresponds to the mSUGRA model. Here, the spectrum shows the well-known feature that the colored sparticles (squarks and gluinos)

³We will henceforth not explicitly specify the scale of the gaugino mass parameters, but this should be clear from the context whether we are referring to the parameters at the weak or at the GUT scale.

are split from, and much heavier than, the lighter uncolored sparticles. As M_3 decreases from 500 GeV, the gluino, and via RGE effects also squark, masses drop giving rise to the “compressed SUSY” mass spectrum. The \tilde{t}_1 squark is the lightest of the squarks, owing to Yukawa coupling and intra-generational mixing effects, and its mass drops below $m_{\tilde{Z}_2}$ and $m_{\tilde{\tau}_1}$ around $M_3 \sim 300$ GeV. We note that the diminished squark masses feed into the Higgs soft masses via the RGEs, and give rise to a falling μ parameter as M_3 drops. The end of parameter space occurs at $M_3 \sim 238$ GeV, where the \tilde{t}_1 becomes the LSP, and so is excluded by limits on stable charged or colored relics from the Big Bang. We see that not only $m_{\tilde{Z}_1}$, but also $m_{\tilde{Z}_2}$, is significantly smaller than μ even at the lower end of M_3 where the WMAP constraint is satisfied, so though \tilde{Z}_1 develops a significantly larger higgsino component compared to mSUGRA where it retains its bino-like character.

In Fig. 1b), we show the neutralino relic density $\Omega_{\tilde{Z}_1} h^2$ versus M_3 for the same parameters as in frame a), using the IsaReD program[11]. For the mSUGRA case of $M_3 = 500$ GeV, $\Omega_{\tilde{Z}_1} h^2 \sim 1.5$, so that the model would be cosmologically excluded, at least if we assume thermal relics and standard Big Bang cosmology. As M_3 decreases from 500 GeV, $\Omega_{\tilde{Z}_1} h^2$ drops slowly until below $M_3 \sim 300$ GeV a more rapid fall-off brings $\Omega_{\tilde{Z}_1} h^2$ into accord with the WMAP measurement, which occurs for $M_3 \sim 255$ GeV. At this point, the \tilde{t}_1 is rather light, with $m_{\tilde{Z}_1} \sim 200$ GeV, and $m_{\tilde{t}_1} \sim 230$ GeV.

In Fig. 2, we show the integrated thermally weighted neutralino annihilation cross sections times relative velocity versus M_3 as obtained using IsaReD, for various neutralino annihilation and co-annihilation processes. Here, x is the temperature in units of the LSP mass. The neutralino relic density is determined by the inverse of the sum shown by the solid red line, so that large annihilation cross sections yield low relic densities. In the mSUGRA case with $M_3 = 500$ GeV, the neutralino annihilation rate is dominated by annihilation to leptons via t -channel slepton exchange. As M_3 decreases, the squark masses, and especially the \tilde{t}_1 mass, decrease, so that $\tilde{Z}_1 \tilde{Z}_1 \rightarrow t\bar{t}$ becomes increasingly important, and in fact dominates the annihilation rate for $240 \text{ GeV} < M_3 < 340 \text{ GeV}$. For lower M_3 values, the $\tilde{t}_1 - \tilde{Z}_1$ mass gap is below 30 GeV, and top-squark co-annihilation then dominates, although in this narrow range $\Omega_{\tilde{Z}_1} h^2$ does not saturate the measured CDM relic density. We also see that as M_3 decreases, annihilation to WW , ZZ and hh also increase in strength due to the lower μ value, and increasing higgsino component of the neutralino⁴. However, these channels never dominate in this case.

In compressed SUSY, a light top squark is desirable in that it enhances the neutralino annihilation rate, and brings the relic density prediction into accord with observation, providing yet another mechanism for reconciliation of the predicted DM relic density with observation. However, generically a light top squark also enhances SUSY loop contributions to the decay $b \rightarrow s\gamma$ [12]. In Fig. 3, we show the branching fraction $BF(b \rightarrow s\gamma)$ vs. M_3 for the same parameters as in Fig. 1. In the mSUGRA case, the predicted branching fraction is in accord with the measured value: $BF(b \rightarrow s\gamma) = (3.55 \pm 0.26) \times 10^{-4}$ from a combination of CLEO, Belle and BABAR data[13]. However, the light \tilde{t}_1 in the low M_3 region reduces

⁴We have traced the turnover at low M_3 in the various curves to a drop in the freeze out temperature that determines the range of integration.

the branching fraction well below the measured value. Of course, this branching fraction is also sensitive to other model parameters, *e.g.* $\tan\beta$. The point, however, is that for the light \tilde{t}_1 case, the SUSY contribution is generically comparable to the SM contribution, so that these must fortuitously combine to be consistent with the experimental value, which itself is in good agreement with the SM prediction. At the very least, in the absence of any real theory of flavor, (such fortuitous) agreement with the measured value, which agrees well with the SM prediction [14] $BF(b \rightarrow s\gamma) = (3.29 \pm 0.33) \times 10^{-4}$, can always be obtained by allowing a small flavor violation in the soft parameter matrices at the GUT scale.

2.1 Scenario A: dark matter searches

Next, we investigate prospects for dark matter searches for the case A model line. We first calculate the spin-independent neutralino-proton scattering cross section using IsaReS[15], and plot the results in Fig. 4a). In the case of mSUGRA at $M_3 = 500$ GeV, the cross section $\sigma_{SI}(\tilde{Z}_1 p) \sim 10^{-10}$ pb, which is near the projected limit of future ton-scale noble liquid dark matter detectors. As M_3 decreases, the squark masses also decrease, which increases the neutralino-proton scattering rate, which occurs primarily via squark exchange diagrams. Furthermore, a reduced value of $|\mu|$ is obtained for the low value of $|M_3|$, resulting in an increased higgsino component of \tilde{Z}_1 (which still remains bino-like) so that the contribution to the direct detection cross section via the Higgs exchange diagram is correspondingly increased. By the time we reach $\Omega_{\tilde{Z}_1} h^2 \sim 0.1$ at $M_3 \sim 255$ GeV, the direct detection cross section has grown by an order of magnitude, to just above 10^{-9} pb. This is a general feature of models with a low M_3 value[5]: for a given (bino-like) neutralino mass, direct detection rates are enhanced in the low M_3 case.

In Fig. 4b), we show the flux of muons expected to be measured at a neutrino telescope from neutralino annihilation into muon neutrinos in the core of the sun. In this and other indirect detection rates, we have implemented the Isajet/DarkSUSY interface[16]. We require muons to have energy $E_\mu > 50$ GeV, the threshold for the IceCube detector[17]. In this case, the rate is again enhanced in going from mSUGRA to compressed SUSY, primarily because of the diminution of squark mass and the reduced value of $|\mu|$ as already discussed above: these increase the spin-dependent neutralino-nucleon scattering cross section and enhance the IceCube rate because of the increased capture of neutralinos by the sun. In the WMAP-allowed region, the neutralinos mainly annihilate to $t\bar{t}$ pairs, so that the energy of the neutrino from top decays is shared with the accompanying b and the daughter muon. We see that although the flux of muon neutrinos corresponding to $E_\mu > 50$ GeV increases by a factor of ~ 500 in going from mSUGRA to the compressed SUSY case illustrated here, the flux of muon neutrinos is still below the reach of IceCube, primarily because the neutralino is still mostly bino-like.

For positrons and anti-protons, we evaluate the averaged differential antiparticle flux in a projected energy bin centered at a kinetic energy of 20 GeV, where we expect optimal statistics and signal-to-background ratio at space-borne antiparticle detectors[18]. We take the experimental sensitivity to be that of the Pamela experiment after three years of data-taking as our benchmark[19]. The expected fluxes depend on the (unknown) details of the neutralino distribution in our galactic halo. Here, we assume a scenario where baryon

infall causes progressive deepening of the gravitational potential well, and a clumpy halo distribution is obtained: the Adiabatically Contracted $N03$ Halo Model[20]

In Fig. 5 we show the expected positron flux in frame *a*) and the expected anti-proton flux in frame *b*) versus M_3 for the same parameters as in Fig. 1. We see that in each case the antimatter flux jumps by a factor of $\sim 10^2$ in going from mSUGRA to compressed SUSY, largely due to the enhanced annihilation rate into $t\bar{t}$ pairs, and the concomitant hard spectrum of e^+ s and \bar{p} s that ensue. In the case shown, the positron flux for compressed SUSY is somewhat below the Pamela reach, while the \bar{p} flux is near the Pamela reach. We warn the reader that for the smooth Burkert halo profile [21] the signals are significantly smaller and beyond the sensitivity of Pamela.

We have also evaluated the average differential anti-deuteron flux in the $0.1 < T_{\bar{D}} < 0.25$ GeV range, where $T_{\bar{D}}$ stands for the antideuteron kinetic energy per nucleon, and compared it to the estimated sensitivity of GAPS for an ultra-long duration balloon-borne experiment[22]. We see in Fig. 6*a*) that the antideuteron flux is again enhanced by a factor of $\sim 10^2$ in going from mSUGRA to compressed SUSY, and in fact moves above the detectability limit of the GAPS experiment. For the Burkert halo profile, the estimated flux for the WMAP-allowed range of M_3 is essentially at the edge of detectability.

Indirect detection of neutralinos is also possible via the detection of high energy gamma rays[23] produced by neutralino annihilation in the center of our Galaxy[24]. These will also be searched for by the GLAST collaboration [25]. We have evaluated expectations for the integrated continuum γ ray flux above an $E_\gamma = 1$ GeV threshold versus M_3 in Fig. 6*b*). These projections are extremely sensitive to the assumed neutralino halo distribution, and drop by more than four orders of magnitude for the Burkert halo profile. This makes it difficult to make any definitive statement about the detectability of this signal (which could serve to map the halo profile rather than a diagnostic of the nature of the DM particle). However, once again we see a factor of ~ 100 enhancement in detection rate in moving from the mSUGRA case where $M_3 = 500$ GeV to the compressed SUSY case with $M_3 \sim 255$ GeV.

2.2 Scenario A: LHC searches

As Martin notes[2], the compressed SUSY mass spectra are generally too heavy for successful sparticle searches at the Fermilab Tevatron. However, (1.1) implies an upper bound on the bino mass, and since we *reduce* M_3 from its unified value, implies that gluinos must be relatively light so that multi-jet + multilepton + E_T^{miss} events from SUSY should be produced in abundance at the CERN LHC, due to turn on in 2008. In this section, we investigate the collider signals expected after cuts for various signal topologies at the LHC.

At the CERN LHC, gluino and squark pair production will be the dominant SUSY production reactions. Gluino and squark production will be followed by their cascade decays[26], resulting in a variety of events with jets, isolated leptons and missing energy. A large number of signals emerge, and can be classified by the number of isolated leptons present. The signal channels we examine include *i.*) no isolated leptons plus jets plus E_T^{miss} (0ℓ), *ii.*) single isolated lepton plus jets plus E_T^{miss} (1ℓ), *iii.*) two opposite sign isolated

leptons plus jets plus E_T^{miss} (OS), *iv.*) two same sign isolated leptons plus jets plus E_T^{miss} (SS) and *v.*) three isolated leptons plus jets plus E_T^{miss} (3ℓ).

The reach of the CERN LHC for SUSY has been estimated for the mSUGRA model in Ref. [27, 28] for low values of $\tan\beta$ and in Ref. [29] for large $\tan\beta$ values. We adopt the cuts and background levels presented in Ref. [27] for our analysis of the signal channels listed above. Hadronic clusters with $E_T > 100$ GeV and $|\eta(\text{jet})| < 3$ within a cone of size $R = \sqrt{\Delta\eta^2 + \Delta\phi^2} = 0.7$ are classified as jets. Muons and electrons are classified as isolated if they have $p_T > 10$ GeV, $|\eta(\ell)| < 2.5$, and the visible activity within a cone of $R = 0.3$ about the lepton direction is less than $E_T(\text{cone}) = 5$ GeV.

Following Ref. [27], we required that the jet multiplicity, $n_{\text{jet}} \geq 2$, transverse sphericity $S_T > 0.2$, $E_T(j_1)$, and further, that $E_T(j_2) > E_T^c$ and $E_T^{\text{miss}} > E_T^c$, where the cut parameter E_T^c is chosen to roughly optimize the signal from gluino and squark production. For the leptons we require $p_T(\ell) > 20$ GeV ($\ell = e$ or μ) and $M_T(\ell, E_T^{\text{miss}}) > 100$ GeV for the 1ℓ signal. For the OS, SS and 3ℓ channels, we require that the two hardest leptons have $p_T \geq 20$ GeV. We have also applied a cut on the transverse plane angle $\Delta\phi(\vec{E}_T^{\text{miss}}, j_c)$ between \vec{E}_T^{miss} and closest jet: $30^\circ < \Delta\phi < 90^\circ$, in the case of the E_T^{miss} channel, *i*).

Our results are shown in Fig. 7 for a rather loose choice of the cut parameter $E_T^c = 100$ GeV. We see that as M_3 decreases from the mSUGRA value of 500 GeV, the signal cross sections increase. The increase is mainly due to increased total gluino and squark production cross sections, due to their decreasing masses. When we reach the DM-allowed compressed SUSY spectrum at $M_3 \sim 250$ GeV, however, the leptonic signals suffer a steep drop-off, while the $E_T^{\text{miss}} + \text{jets}$ signal increases somewhat. This is due to the fact that in this case, $\widetilde{W}_1 \rightarrow b\tilde{t}_1$ turns on and dominates the \widetilde{W}_1 branching fraction, while $\tilde{t}_1 \rightarrow c\tilde{Z}_1$ at essentially 100%. Thus, no isolated leptons come from chargino decay. Likewise, $\tilde{Z}_2 \rightarrow \tilde{Z}_1 h$ at around 90% branching fraction, so isolated leptons from \tilde{Z}_2 decays come from the subdominant decay chain $\tilde{Z}_2 \rightarrow \tilde{Z}_1 Z$ which has a branching fraction of $\sim 8\%$. Isolated leptons still arise from $\tilde{g} \rightarrow t\tilde{t}_1$ decay, followed by semi-leptonic top decay, but in general, we expect in compressed SUSY models with a small $\tilde{t}_1 - \tilde{Z}_1$ mass gap and $m_{\widetilde{W}_1} > m_{\tilde{t}_1} + m_b$ that the fraction of signal events containing isolated leptons will be much *lower* than the usual prediction from models like mSUGRA with gaugino mass unification. We regard a signal to be observable if for the given integrated luminosity, *i*) the statistical significance of the signal exceeds 5σ , *ii*) $S/B > 0.25$, and *iii*) $S > 10$ events. The minimum observable cross sections for each topology are shown by the dashed horizontal bars in the figure. We see that even for the low value of $E_T^c = 100$ GeV, all but the opposite sign dilepton signal should be observable with an integrated luminosity of 100 fb^{-1} , and frequently even with a much lower integrated luminosity, at least for parameters in the WMAP-allowed region. Although we do not show this, we have checked that with $E_T^c = 200$ GeV, the OS signal is easily observable,⁵ and furthermore, the 0ℓ signal is not as close to the observability limit.

⁵Since the OS dileptons come primarily from the decay of an on-shell Z boson, it is possible that this signal would actually be observable even for $E_T^c = 100$ GeV.

3. Case B: Non-universal gaugino masses and a large mass gap

In this section, we explore Case B, the compressed SUSY model line originally suggested by Martin where at $Q = M_{\text{GUT}}$, $1.5M_1 = M_2 = 3M_3$, with $m_0 = 340$ GeV, $A_0 = -0.75M_1$, $\tan\beta = 10$ and $\mu > 0$. We first display the variation of the sparticle mass spectrum with M_1 in Fig. 8a). The upper end of parameter space is limited by $M_1 \lesssim 1000$ GeV, where for higher M_1 values the \tilde{t}_1 becomes the LSP. This implies an upper bound of 1200 GeV (1100–1400 GeV) on gluino (squark) masses, ensuring their copious production at the LHC. The lower range of M_1 is bounded by $M_1 \gtrsim 160$ GeV, since for lower M_1 values, the value of $m_{\tilde{W}_1}$ drops below limits from LEP2 [30]. In the intermediate region with 440 GeV $< M_1 < 1000$ GeV, the \tilde{t}_1 is relatively light, and is the next-to-lightest SUSY particle (NLSP). More importantly from our perspective, in this mass regime $m_{\tilde{Z}_1} > m_t$, ensuring that $\tilde{Z}_1\tilde{Z}_1 \rightarrow t\bar{t}$ was accessible in the early Universe.

In Fig. 8b), we show the neutralino relic density as a function of M_1 for the same parameters as in frame a). There is a wide range of $M_1 : 400 - 800$ GeV where the relic abundance is in close accord with the WMAP measured value. It should be possible to bring this in accord with the WMAP value by slightly tweaking A_0 . For yet larger values of M_1 , $\tilde{t}_1\tilde{Z}_1$ and $\tilde{t}_1\tilde{t}_1$ annihilation rates become large, and the \tilde{Z}_1 relic density no longer saturates the observed density of CDM; *i.e.* the DM would be multi-component in this case. In contrast, when M_1 drops below ~ 400 GeV, corresponding to $m_{\tilde{Z}_1} < m_t$, the prediction for $\Omega_{\tilde{Z}_1} h^2$ rises above the WMAP measurement, excluding \tilde{Z}_1 as a thermal relic. For $M_1 \sim 150$ GeV – a range excluded by the LEP2 chargino mass limit – there is a double dip structure where $2m_{\tilde{Z}_1} \sim m_h$ or M_Z , and so neutralinos can efficiently annihilate through these s -channel poles.

In Fig. 9, we show the integrated thermally weighted neutralino annihilation (and co-annihilation) cross section times relative velocity versus M_1 for the same parameters as in Fig. 8. For $M_1 \gtrsim 750$ GeV, the $\tilde{t}_1 - \tilde{Z}_1$ mass gap is so low that $\tilde{Z}_1\tilde{t}_1$ co-annihilation, and eventually $\tilde{t}_1\tilde{t}_1$ annihilation (not shown in the figure), dominates and we get too small a relic abundance. In the range 400 GeV $\lesssim M_1 \lesssim 750$ GeV, $\tilde{Z}_1\tilde{Z}_1 \rightarrow t\bar{t}$ dominates, so agreement with the relic density is obtained as envisioned by Martin [2]. For $M_1 \lesssim 400$ GeV, annihilation into $t\bar{t}$ is not allowed (except for \tilde{Z}_1 s in the high energy tail of the thermal distribution), and so annihilation takes place dominantly into WW (via the higgsino component) and into quarks and leptons. At the h and Z poles (inside the LEP-forbidden region), annihilation into down-type fermions dominates.

The branching fraction $BF(b \rightarrow s\gamma)$ is shown in Fig. 10 versus M_1 for the same parameters as in Fig. 8. Here we note that for large M_1 , the branching fraction is close to–albeit somewhat below–its measured value. However, as M_1 decreases, the \tilde{t}_1 and \tilde{W}_1 both become lighter, and SUSY loop contributions to the branching fraction move the predicted branching fraction away from its observed value. In this case, as in Sec. 2, we would expect a somewhat suppressed value of $BF(b \rightarrow s\gamma)$ compared to its SM predicted rate. We recall as before that it should be possible to bring this result into accord with experiment by allowing, for instance, some flavor structure in the soft SUSY breaking sector.

3.1 Case B: dark matter searches

Here, we examine direct and indirect dark matter detection rates for the compressed SUSY model line Case B. We begin by considering the prospects for direct detection in Fig. 11a) where we show the spin-independent $\tilde{Z}_1 p$ cross section as a function of the GUT scale parameter M_1 . The cross section increases as M_1 decreases due to decreasing squark masses, and a decreasing value of the μ parameter. The range relevant for compressed SUSY, $M_1 : 400 - 750$ GeV, has $\sigma_{SI}(\tilde{Z}_1 p) \sim 5 - 15 \times 10^{-9}$ pb, which at its high end is within an order of magnitude of the current limit from XENON-10[31], and should be detectable by SuperCDMS or 100-1000 kg noble liquid DM detectors. Projections for direct detection are somewhat more optimistic than in Case A, mostly because the value of μ is relatively smaller in Case B.

In frame b), we show the flux of muons with $E_\mu > 50$ GeV expected at neutrino telescopes due to neutralino annihilation in the solar core. As M_1 decreases from 1000 GeV, the rate slightly increases, due to an increasing spin-dependent \tilde{Z}_1 -nucleon scattering rate, but for the M_1 range of interest, the flux remains somewhat below the IceCube detectable level. For $M_1 < 400$ GeV, the rate jumps to higher levels. This jump can be understood from Fig. 9, from which we infer that since the neutralino capture and annihilation processes are in equilibrium, the fraction of captured neutralinos that directly annihilate into $\nu\bar{\nu}$ jumps once annihilation to $t\bar{t}$ turns off, and it is these very high energy neutrinos which have the greatest chance of being detected by IceCube. For $M_1 > 400$ GeV, $\tilde{Z}_1\tilde{Z}_1$ annihilates mainly into $t\bar{t}$, and the fraction of direct neutralino annihilation into neutrinos is lower.

In Fig. 12 we show the flux of a) positrons and b) anti-protons from neutralino annihilations in the galactic halo expected in Case B versus M_1 , assuming the clumpy halo as given by the adiabatically contracted N03 halo model. We evaluate the signal in the same energy bins and apply the same sensitivity criterion as in Fig. 5. The flux of e^+ s is everywhere below the Pamela sensitivity even for our favorable choice of halo distribution. However, the results do show some structure and enhancement in the compressed SUSY range of $M_1 : 440 - 800$ GeV. In this regime, $m_{\tilde{Z}_1} > m_t$ so that $\tilde{Z}_1\tilde{Z}_1 \rightarrow t\bar{t}$ can occur in the present galactic halo as well as in the early Universe. The turn-on of the $t\bar{t}$ annihilation mode is clearly seen at $M_1 \sim 440$ GeV. In the case of the \bar{p} flux, the signal actually increases enough to suggest some range of observability at Pamela.

In Fig. 13 we show a) the flux of anti-deuterons along with the reach of the GAPS experiment, and b) the flux of gamma rays from the galactic center with $E_\gamma > 1$ GeV. In the case of \bar{D} s, the entire compressed SUSY range is above the GAPS sensitivity. We caution, however, that for the smooth Burkert halo profile, projections could be lower by a factor 10-15. For γ s, the entire range should be probed by GLAST, although these projections are extremely sensitive to our assumed halo distribution; for other halo choices – such as the Burkert profile, the rates scale downwards by over four orders of magnitude, and could fall below the projected sensitivity of GLAST. However, in both the case of \bar{D} s and γ s, a sharp increase in indirect detection rate occurs when $\tilde{Z}_1\tilde{Z}_1 \rightarrow t\bar{t}$ turns on at $M_1 \sim 440$ GeV.

3.2 Scenario B: LHC searches

An important issue for evaluating collider signals in compressed SUSY with a large $\tilde{t}_1 - \tilde{Z}_1$ mass gap is to evaluate the \tilde{t}_1 decay branching fractions correctly when the \tilde{t}_1 is the NLSP. In this case, the flavor changing decay $\tilde{t}_1 \rightarrow c\tilde{Z}_1$ may compete with the three-body decay $\tilde{t}_1 \rightarrow bW\tilde{Z}_1$ if the latter decay mode is kinematically allowed. We implement the three body decay into Isajet 7.76 using the squared matrix element calculated by Porod and Wöhrmann[32].⁶ We also update the Isajet formulae for the flavor changing two-body decay using the one-step integration approximation of Hikasa and Kobayashi[34], but with the correct neutralino eigenvectors [35]. We have checked that this single step integration systematically over-estimates the width of the loop decay $\tilde{t}_1 \rightarrow c\tilde{Z}_1$, so that if we find the three body decay to be dominant within our approximation, this will be the case also with the correct calculation. In Fig. 14, we show the branching fraction of \tilde{t}_1 versus M_1 for the same parameters as in Fig. 8. We see that at large M_1 where $m_{\tilde{t}_1} < m_b + M_W + m_{\tilde{Z}_1}$, the \tilde{t}_1 decays entirely into $c\tilde{Z}_1$ ⁷. For lower M_1 values, the $\tilde{t}_1 \rightarrow bW\tilde{Z}_1$ decay mode opens up and in fact dominates the two-body mode for $M_1 : 400 - 460$ GeV. For $M_1 \lesssim 400$ GeV, then $m_{\tilde{t}_1} > m_b + m_{\tilde{W}_1}$, so that $\tilde{t}_1 \rightarrow b\tilde{W}_1$ turns on and dominates the branching fraction. In this regime, for this case at least, $m_{\tilde{Z}_1} < m_t$, so this range is not as interesting from the perspective of obtaining agreement with the relic density measurement via neutralino annihilation to top quarks.

Once the correct decay patterns are implemented, we can generate collider events and examine signal rates after cuts. We present multi-lepton plus multi-jet $+E_T^{\text{miss}}$ cross sections at the LHC for Case B, using the same analysis as in Sec. 2.2, except with $E_T^c = 200$ GeV. The results are shown in Fig. 15. For low M_1 values, the squark and gluino masses are relatively light, and SUSY particle production cross sections are large at the CERN LHC. Nevertheless, signals in the 0ℓ , 1ℓ and OS channels fall below the $S/B \geq 0.25$ level for M_1 in the interesting range of 400-800 GeV if we choose $E_T^c = 100$ GeV. In contrast, with $E_T^c = 200$ GeV shown in the figure, signals in all channels are observable for the entire range of M_1 .⁸ As M_1 increases, the $\tilde{g} - \tilde{W}_1$ and $\tilde{q} - \tilde{W}_1$ mass gaps actually increase, and we get an increase in the multi-lepton signal rates. These show a rapid drop off beyond $M_1 = 450$ -500 GeV, where \tilde{t}_1 produced in gluino cascades decay via $\tilde{t}_1 \rightarrow c\tilde{Z}_1$. There is no analogous drop-off in the 0ℓ or even in the 1ℓ channels (since it is not difficult to get a single lepton somewhere in the cascade, *e.g.* via the decay of t). Thus, once the stop is light enough so it can only decay via $\tilde{t}_1 \rightarrow c\tilde{Z}_1$ (which is the case over most of the M_1 range of interest), we see a relative reduction of multi-leptonic signals compared with those containing just $E_T^{\text{miss}} + \text{jets}$. Distinguishing Case B (with $\tilde{t}_1 \rightarrow c\tilde{Z}_1$) from Case A will be challenging at the LHC, but should be straightforward at a TeV linear collider.

⁶We have, however, made one correction from their erratum. The term $2m_{\tilde{Z}_1}^2 (2p_b \cdot p_W + m_{\tilde{Z}_1}^2)$ in Eq. (A.2) should be replaced by $2m_{\tilde{Z}_1}^2 p_b \cdot p_W$ and not by $4m_{\tilde{Z}_1}^2 p_b \cdot p_W$ as stated in their erratum. M. Mühlleitner (private communication) has independently confirmed this factor, which also appears correctly in the program SDECAY[33].

⁷There are four body decay modes such as $\tilde{t}_1 \rightarrow bf\tilde{f}'\tilde{Z}_1$ (where f is a SM fermion) which we have not evaluated, but which we expect to be smaller than the two-body decay[36].

⁸The $E_T^c = 100$ GeV is better optimized for the signals in the SS and 3ℓ channels.

4. Summary and conclusions

The *generic* prediction of the neutralino relic density from SUSY models falls somewhat above the measured value if sparticles are significantly heavier than ~ 100 GeV, as is likely to be the case given the direct constraints from LEP2 and the Tevatron, and indirect constraints from low energy measurements. Within a particular framework such as mSUGRA, this means special regions of parameter space where at least one of: neutralino co-annihilation with staus/stops, neutralino resonance annihilation via A/H (this requires large $\tan\beta$ values) or even h , or mixed higgsino DM in the hyperbolic branch/focus point region at large m_0 , obtains. Each of these alternatives would have implications for SUSY signals both at colliders, as well as for direct and indirect searches for DM. Unfortunately, these implications are not robust to small changes in the model. Allowing for non-universality of gaugino or Higgs scalar mass parameters leads to one-parameter extensions of the mSUGRA model where the implications of the WMAP measurement can be strikingly different. For instance, non-universal Higgs mass models allow mixed Higgsino DM for low values of m_0 , and Higgs resonance annihilation for all values of $\tan\beta$ [37]. Non-universal gaugino masses allow new possibilities, such as mixed wino DM [38] or bino-wino co-annihilation [39] that are precluded in models with unified gaugino masses (but realized in other frameworks). These studies suggest that it would be premature to blindly use the measured relic density to make definitive projections for what should/should not be seen at the LHC or in DM searches. Already there exist numerous alternatives (with different phenomenological outcomes) to choose from, and only experiment can zero in on nature's choice.

In this vein, Martin [2] recently pointed out yet another possibility to obtain agreement with the observed CDM relic density. He noted that if $m_{\tilde{Z}_1} > m_t$ and \tilde{t}_1 is not much heavier than \tilde{Z}_1 , then $\tilde{Z}_1\tilde{Z}_1 \rightarrow t\bar{t}$ mediated by \tilde{t}_1 exchange (this process does not suffer the large p -wave suppression on account of the large top mass) may dominate in the early universe. This scenario can be realized for a bino-like \tilde{Z}_1 only if gluinos (and through the RGEs, also the squarks) are not very heavy, leading to a ‘‘compressed SUSY’’ spectrum. In this paper, we have examined two different model lines that realize Martin's idea, and quantified the implications for SUSY searches at the LHC as well as via direct and indirect searches for DM.

The first model line that we refer to as Case A is continuously connected to mSUGRA, and is in a sense an extension of our earlier work that we referred to as low $|M_3|$ dark matter, where relaxing the gaugino mass unification condition and allowing $|M_3(\text{GUT})|$ to be smaller than $M_1 \sim M_2$ led to viable solutions with mixed higgsino DM [5]. In these studies, we used $A_0 = 0$ for simplicity. Here, we choose instead $A_0 = -1.5m_{1/2}$, and lower M_3 as before. This choice of A_0 leads to a reduction in $m_{\tilde{t}_1}$, and remarkably, as M_3 is reduced, $m_{\tilde{t}_1}$ becomes close to $m_{\tilde{Z}_1}$, so that $\tilde{Z}_1\tilde{Z}_1 \rightarrow t\bar{t}$ can indeed be the dominant mechanism in the early Universe, with \tilde{Z}_1 retaining its bino-like character. While the reduced gluino, and concomitantly squark, masses and the μ parameter, imply larger direct and indirect detection rates *vis à vis* models with gaugino mass unification, these rates are not large, primarily because the neutralino remains bino-like. Nevertheless ton size noble

liquid detectors should be able to directly see a WIMP signal (at least for parameters that give the observed relic density), while indirect searches for anti-deuteron at GAPS or gamma rays from our galactic center by GLAST may yield an observable signal, but only if the DM is favorably clumped. We project that there will be no detectable signal in Pamela or in IceCube. The scenario implies that gluinos and squarks cannot be too heavy so that the LHC should be awash in SUSY events, and the signal should be extricable from SM backgrounds with simple cuts. The characteristic feature of the scenario is the relative reduction of the signal in multi-lepton channels relative to that in 0ℓ or 1ℓ channels. The large production rate nevertheless implies there should be an observable signal in *all* the channels shown in Fig. 7. A significant fraction of OS dilepton and trilepton events may contain a real Z boson.

The second model line that we examine (and refer to as Case B) is the one suggested by Martin in his original proposal. Here, we adopt non-universal boundary conditions $1.5M_1 = M_2 = 3M_3$ for the GUT scale gaugino mass parameters. Prospects for direct detection may be somewhat better in this scenario: in favorable cases, the signal cross section may be just an order of magnitude away from the current upper bound. Indirect detection prospects are similar to those in Case A. There is no detectable signal at IceCube, potentially observable signals in GLAST or GAPS for favorable halo distributions, and possibly a marginal signal from \bar{p} in Pamela. Experiments at the LHC should be able to detect a signal in all channels, albeit with somewhat harder cuts than in Case A, as illustrated in Fig. 15. As in Case A, over most of the parameter range compatible with the relic density measurement, multi-lepton signals will occur at smaller rates.

A light \tilde{t}_1 is the hallmark of the scenario. While its direct detection is not easy at the LHC,⁹ its presence along with that of a not-too-heavy chargino leads to a significant SUSY contribution to the $b \rightarrow s\gamma$ branching ratio, and likely also to the branching ratio and distributions for $b \rightarrow s\ell\bar{\ell}$ decays (that we have not examined). Indeed, for both cases that we examined, the former turns out to be smaller than its measured value. While it is certainly true that we can always reproduce the observed branching fraction by tweaking the flavour structure of soft-SUSY-breaking parameters, it would seem unlikely this would be “just right” to yield the SM prediction. It, therefore, seems that a deviation of the patterns of rare flavor-violating decays of b -quarks from SM expectations should generically be expected in these scenarios.

Acknowledgments

This research was supported in part by the U.S. Department of Energy grant numbers DE-FG02-97ER41022 and DE-FG02-04ER41291.

References

- [1] D. N. Spergel *et al.*, [astro-ph/0603449](#) (2006); see D. N. Spergel *et al.*, [astro-ph/0302209](#) (2003) for results from the analysis of the first year of WMAP data.

⁹The techniques suggested in Ref. [40] do not apply since $\tilde{t}_1 \rightarrow c\tilde{Z}_1$.

- [2] S. P. Martin, *Phys. Rev. D* **75** (2007) 115005.
- [3] G. Belanger, F. Boudjema, A. Cottrant, A. Pukhov and A. Semenov, *Nucl. Phys. B* **706** (2005) 411.
- [4] Y. Mambrini and E. Nezri, *Eur. Phys. J. C* **50** (2007) 949.
- [5] H. Baer, A. Mustafayev, E. K. Park, S. Profumo and X. Tata, *J. High Energy Phys.* **0604** (2006) 041. See also H. Baer, A. Mustafayev, S. Profumo and X. Tata, *Phys. Rev. D* **75** (2007) 035004.
- [6] G. Anderson *et al.* in *New Directions for High Energy Physics*, Proc. Snowmass 1996, V 2, p. 669, D. Cassel, L. Trindle-Gennari and R. H. Siemann, Editors; G. Anderson, H. Baer, C. H. Chen and X. Tata, *Phys. Rev. D* **61** (2000) 095005.
- [7] K. Choi, K-S. Jeong and K. Okumura, *J. High Energy Phys.* **0509** (2005) 039. A. Falkowski, O. Lebedev and Y. Mambrini, *J. High Energy Phys.* **0511** (2005) 034; H. Baer, E. K. Park, X. Tata and T. Wang, *J. High Energy Phys.* **0608** (2006) 041, *Phys. Lett. B* **641** (2006) 447 and [hep-ph/0703024](#). K. Choi, K. Y. Lee, Y. Shimizu, Y. G. Kim and K. Okumura, *JCAP***0612** (2006) 017.
- [8] K. J. Bae, R. Dermisek, H. D. Kim and I. W. Kim, [hep-ph/0702041](#).
- [9] H. Baer and J. O’Farrill, *JCAP***0404** (2004) 005 and H. Baer, A. Belyaev, T. Krupovnickas and J. O’Farrill, *JCAP***0408** (2004) 005.
- [10] ISAJET v7.76, by H. Baer, F. Paige, S. Protopopescu and X. Tata, [hep-ph/0312045](#); see also H. Baer, J. Ferrandis, S. Kraml and W. Porod, *Phys. Rev. D* **73** (2006) 015010.
- [11] H. Baer, C. Balazs and A. Belyaev, *J. High Energy Phys.* **0202** (2002) 042.
- [12] H. Baer and M. Brhlik, *Phys. Rev. D* **55** (1997) 3201; H. Baer, M. Brhlik, D. Castaño and X. Tata, *Phys. Rev. D* **58** (1998) 015007.
- [13] E. Barberio *et al.* (Heavy Flavor Averaging Group), [hep-ex/0603003](#).
- [14] K. Chetyrkin, M. Misiak and M. Munz, *Phys. Lett. B* **400** (1997) 206 and erratum-ibid, *Phys. Lett. B* **425** (1998) 414; A. Buras *et al.*, *Phys. Lett. B* **414** (1997) 157 and erratum-ibid, *Phys. Lett. B* **434** (1998) 459; A. Kagan and M. Neubert, *Eur. Phys. J. C* **7** (1999) 5.
- [15] H. Baer and M. Brhlik, *Phys. Rev. D* **57** (1998) 567; H. Baer, C. Balazs, A. Belyaev and J. O’ Farrill, *JCAP***0309** (2003) 007.
- [16] P. Gondolo, J. Edsjo, P. Ullio, L. Bergstrom, M. Schelke and E. A. Baltz, *JCAP* **0407** (2004) 008
- [17] J. Ahrens *et al.*, (IceCube Collaboration), *Nucl. Phys.* **118** (*Proc. Suppl.*) (2003) 388; F. Halzen, [astro-ph/0311004](#); F. Halzen and D. Hooper, *JCAP***0401** (2004) 002.
- [18] S. Profumo and P. Ullio, *JCAP* **0407** (2004) 006; S. Profumo and C.E. Yaguna, *Phys. Rev. D* **70** (2004) 095004.
- [19] M. Pearce (Pamela Collaboration), *Nucl. Phys.* **113** (*Proc. Suppl.*) (2002) 314.
- [20] J.F. Navarro *et al.*, *MNRAS*, **349** (2004) 1039; B. Moore, *et al.*, *Astrophys. J. Lett.* **524**, L19 (1999).
- [21] A. Burkert, *Astrophys. J.* **447** (1995) L25; P. Salucci and A. Burkert, *Astrophys. J.* **537** (2000) L9.

- [22] K. Mori, C. J. Hailey, E. A. Baltz, W. W. Craig, M. Kamionkowski, W. T. Serber and P. Ullio, *Astrophys. J.* **566** (2002) 604, C. J. Hailey *et al.*, *JCAP* **0601** (2006) 007; H. Baer and S. Profumo, *JCAP***0512** (2005) 008.
- [23] H. A. Mayer-Hasselwander *et al.* (EGRET Collaboration), MPE-440 (1998).
- [24] F. Stecker, *Phys. Lett.* **B 201** (1988) 529; F. W. Stecker and A. J. Tylka, *Astrophys. J.* **343** (1989) 169; S. Rudaz and F. Stecker, *Astrophys. J.* **368** (1991) 406; M. Urban *et al.*, *Phys. Lett.* **B 293** (1992) 149; V. Berezhinsky, A. Gurevich and K. Zybin, *Phys. Lett.* **B 294** (1992) 221; V. Berezhinsky, A. Bottino and G. Mignola, *Phys. Lett.* **B 325** (1994) 136; L. Bergstrom, P. Ullio and J. H. Buckley, *Astropart. Phys.* **9** (1998) 137; L. Bergstrom, J. Edsjö and P. Ullio, *Phys. Rev.* **D 58** (1998) 083507; J. Buckley *et al.*, [astro-ph/0201160](http://arxiv.org/abs/astro-ph/0201160); P. Ullio, L. Bergstrom, J. Edsjö and C. Lacey, *Phys. Rev.* **D 66** (2002) 123502; see also H. Baer, A. Belyaev, T. Krupovnickas and J. O' Farrill, *JCAP***0408** (2004) 005.
- [25] A. Morselli *et al.*, (GLAST Collaboration), *Nucl. Phys.* **113** (*Proc. Suppl.*) (2002) 213.
- [26] H. Baer, J. Ellis, G. Gelmini, D. Nanopoulos and X. Tata, *Phys. Lett.* **B 161** (1985) 175; G. Gamberini, *Z. Physik* **C 30** (1986) 605; H. Baer, V. Barger, D. Karatas and X. Tata, *Phys. Rev.* **D 36** (1987) 96.
- [27] H. Baer, C. H. Chen, F. Paige and X. Tata, *Phys. Rev.* **D 52** (1995) 2746 and *Phys. Rev.* **D 53** (1996) 6241.
- [28] S. Abdullin *et al.* (CMS Collaboration), hep-ph/9806366 (1998); S. Abdullin and F. Charles, *Nucl. Phys.* **B547**, 60 (1999); ATLAS collaboration, Technical Design Report, V II, CERN/LHCC/99-15 (1999); B. Allanach, J. Hetherington, M. Parker and B. Webber, *J. High Energy Phys.* **0008** (2000) 017.
- [29] H. Baer, C. H. Chen, M. Drees, F. Paige and X. Tata, *Phys. Rev.* **D 59** (1999) 055014.
- [30] See *e.g.* Joint LEP SUSY Working Group, <http://lepsusy.web.cern.ch/lepsusy/>
- [31] J. Angle *et al.* (XENON Collaboration) arXiv:0706.0039 (2007).
- [32] W. Porod and T. Wöhrmann, *Phys. Rev.* **D 55** (1997) 2907, and *Phys. Rev.* **D 67** (2003) 059902(E).
- [33] M. Mühlleitner, A. Djouadi and Y. Mambrini, *Comput. Phys. Commun.* **168** (2005) 46.
- [34] K. Hikasa and M. Kobayashi, *Phys. Rev.* **D 36** (1987) 724.
- [35] H. Baer, M. Drees, R. Godbole, J. F. Gunion and X. Tata, *Phys. Rev.* **D 44** (1991) 725; T. Han, K. Hikasa, J. Yang and X-M. Zhang, *Phys. Rev.* **D 70** (2004) 055001.
- [36] C. Boehm, A. Djouadi, Y. Mambrini, *Phys. Rev.* **D 61** (2000) 095006.
- [37] See *e.g.* H. Baer, A. Mustafayev, S. Profumo, A. Belyaev and X. Tata, *J. High Energy Phys.* **0507** (2005) 065, and references therein.
- [38] See *e.g.* H. Baer, A. Mustafayev, E. Park and S. Profumo, *J. High Energy Phys.* **0507** (2005) 046, and references therein.
- [39] H. Baer, T. Krupovnickas, A. Mustafayev, E. Park, S. Profumo and X. Tata, *J. High Energy Phys.* **0512** (2005) 011.
- [40] J. Hisano, K. Kawagoe and M. Nojiri, *Phys. Rev.* **D 68** (2003) 035007.

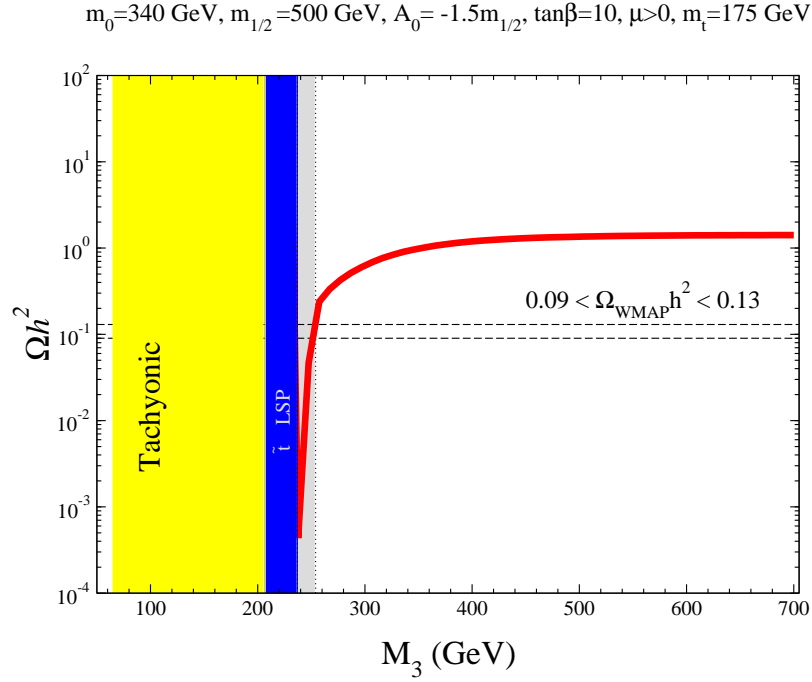
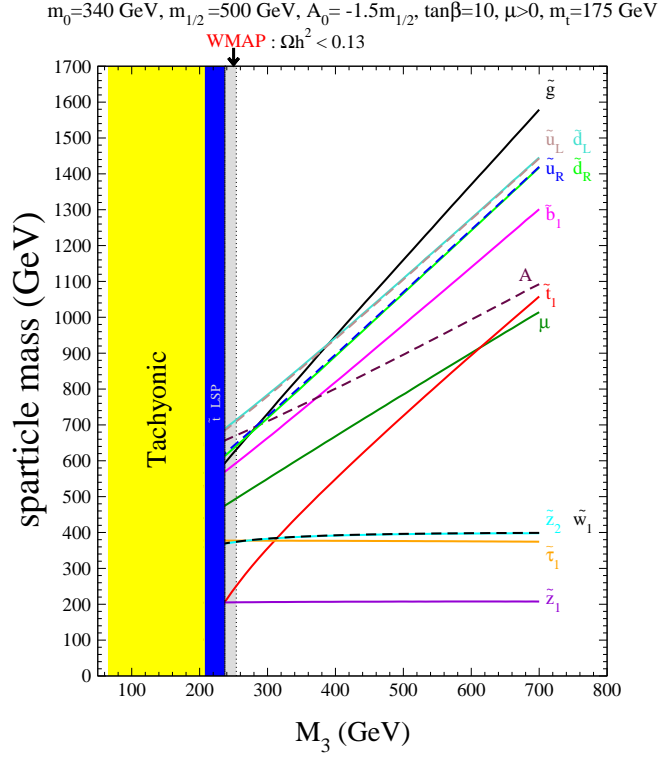


Figure 1: a) Sparticle mass spectrum for the case with $m_0 = 340$ GeV, $M_1 = M_2 = 500$ GeV, $A_0 = -1.5m_{1/2}$, $\tan\beta = 10$, $\mu > 0$ and $m_t = 175$ GeV, versus GUT scale $SU(3)$ gaugino mass parameter M_3 , and b) neutralino relic density versus M_3 for same parameters as in frame a).

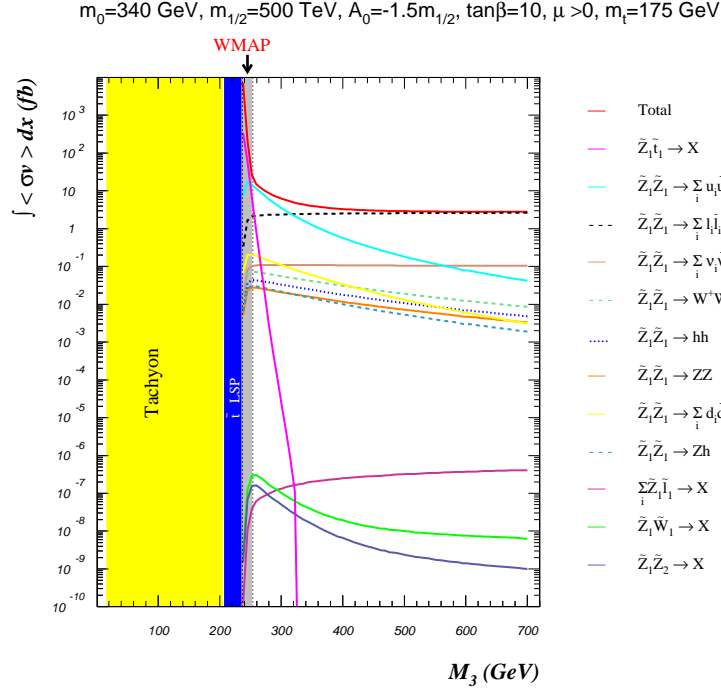


Figure 2: Integrated thermally weighted cross sections times relative velocity for processes that may be relevant for the calculation of the \tilde{Z}_1 relic density in the Big Bang versus M_3 . We illustrate these for the same parameters as in Fig. 1.

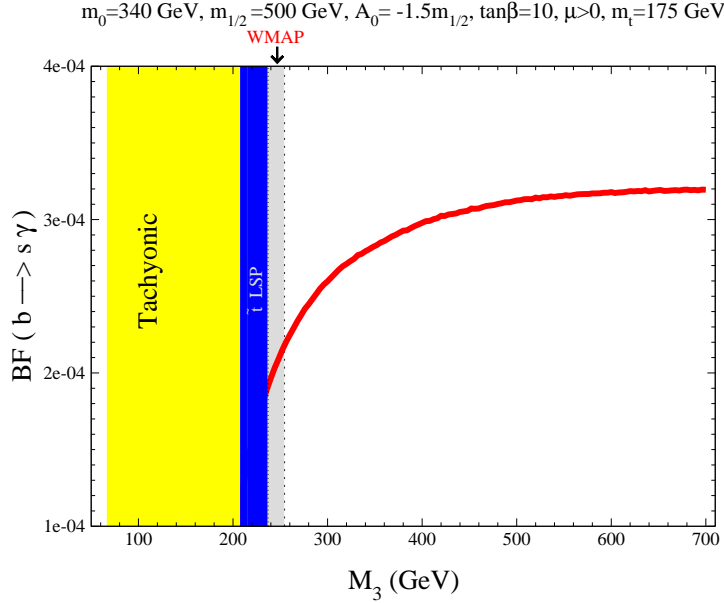


Figure 3: Branching fraction for $b \rightarrow s\gamma$ decay versus M_3 for same parameters as in Fig. 1.

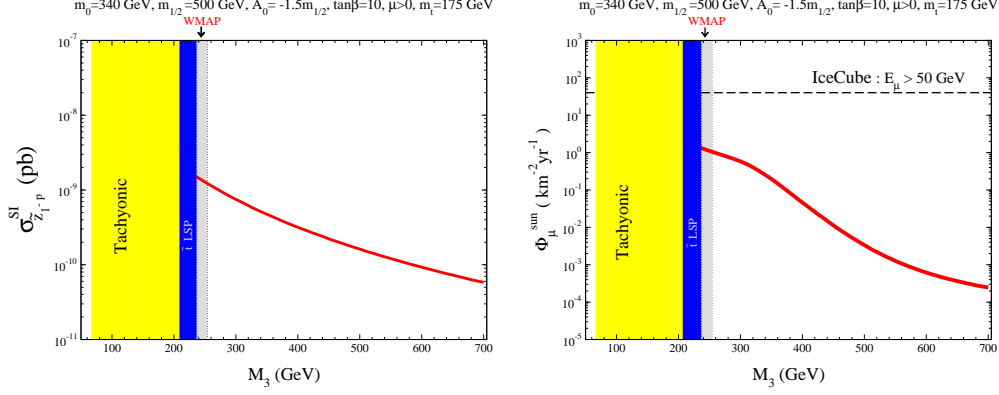


Figure 4: *a)* Spin-independent neutralino-proton scattering cross section and *b)* flux of muons with $E_\mu > 50$ GeV at IceCube versus M_3 for same parameters as in Fig. 1.

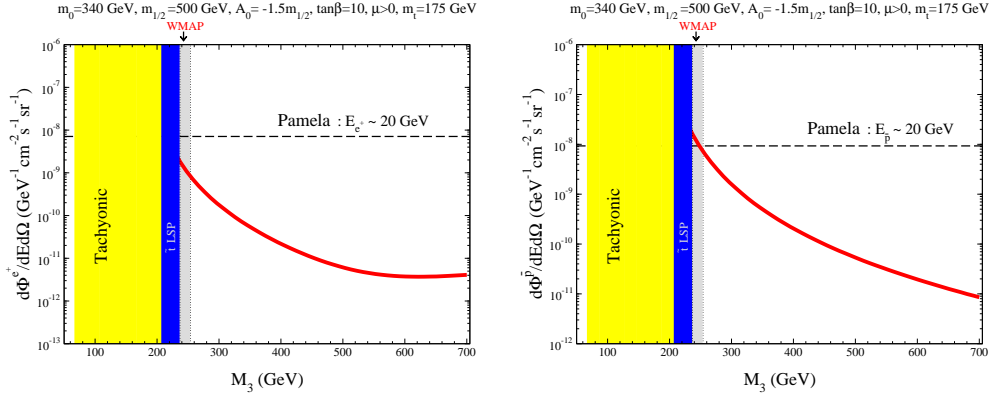


Figure 5: *a)* Expected positron flux and *b)* antiproton flux versus M_3 for same parameters as in Fig. 1. The dashed line shows the expected three year sensitivity of Pamela.

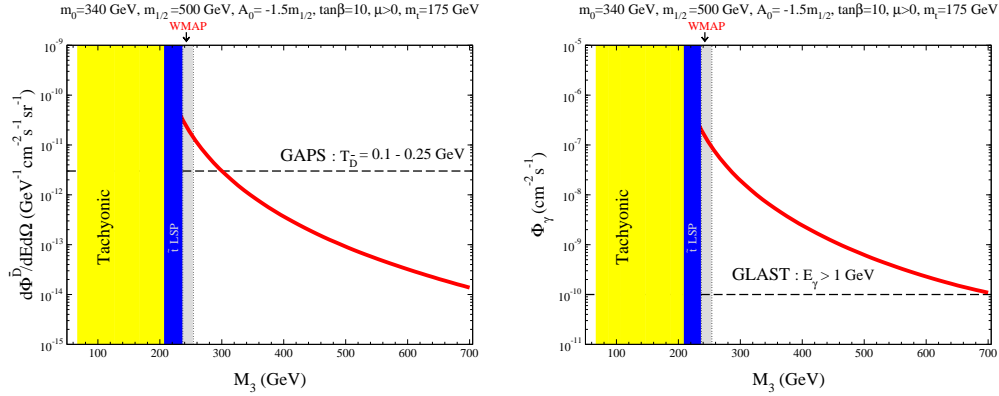


Figure 6: *a)* Expected anti-deuteron flux and *b)* gamma ray flux versus M_3 for same parameters as in Fig. 1. The horizontal lines show the projected sensitivities of the GAPS and GLAST experiments.

$m_0=340$ GeV, $m_{1/2}=500$ GeV, $A_0=-750$ GeV, $\tan\beta=10$, $\mu>0$, $m_t=175$ GeV

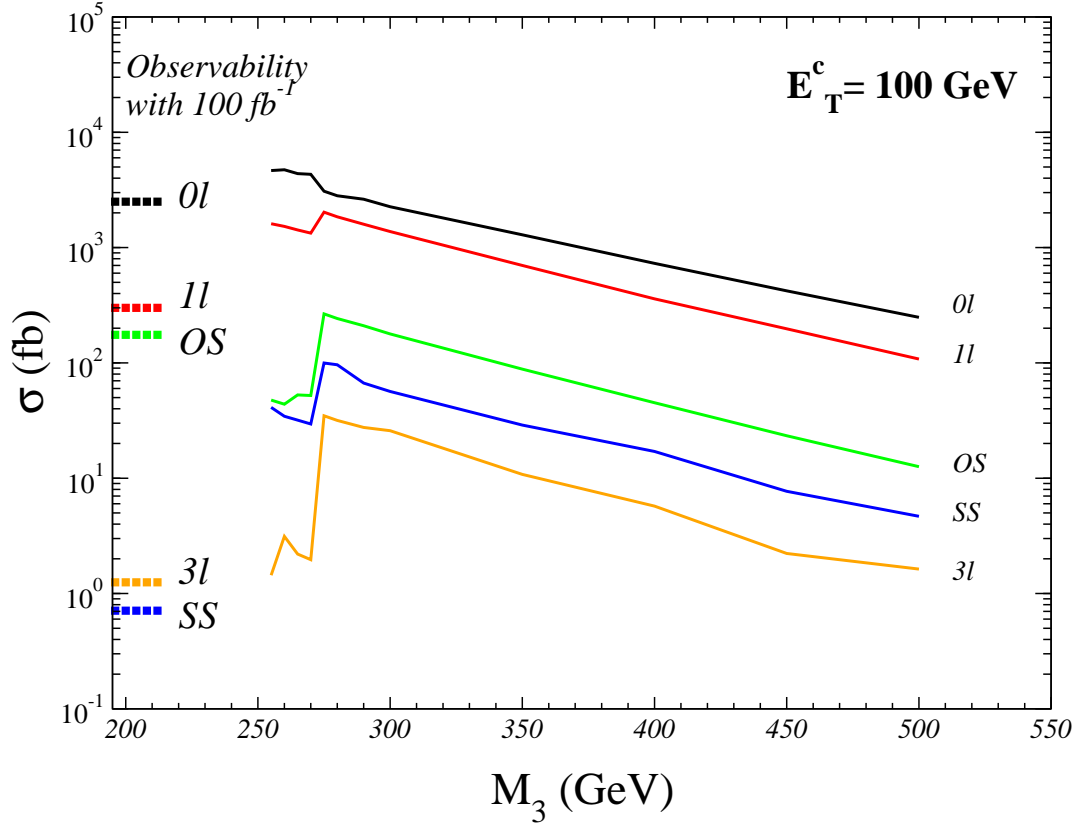


Figure 7: Signal rates at the CERN LHC for various multi-jet plus multi-lepton $+E_T^{\text{miss}}$ event topologies after cuts listed in the text with the cut parameter $E_T^c = 100$ GeV versus M_3 for same parameters as in Fig. 1. The horizontal dotted lines show the minimum observable cross section for $E_T^c = 100$ GeV, assuming an integrated luminosity of 100 fb^{-1} .

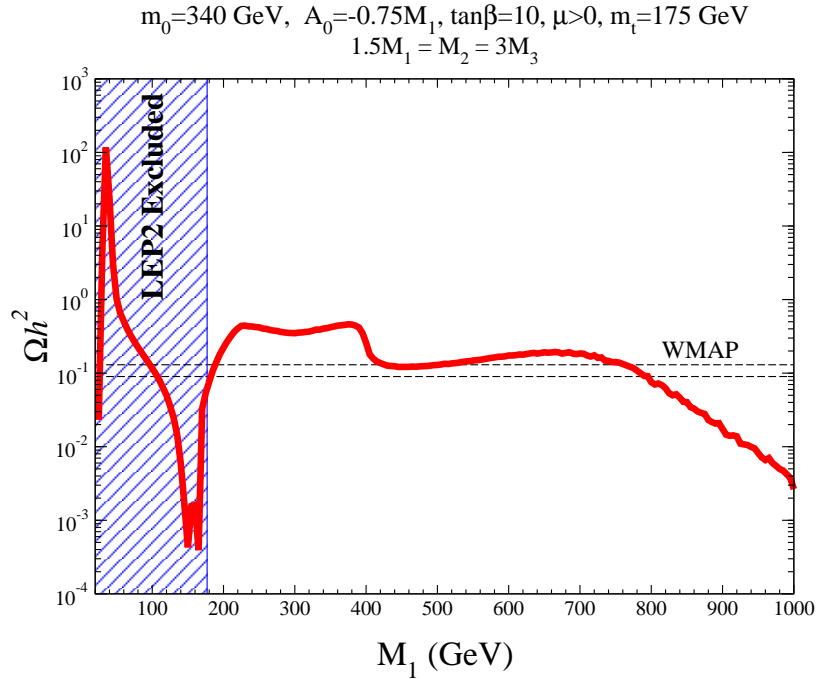
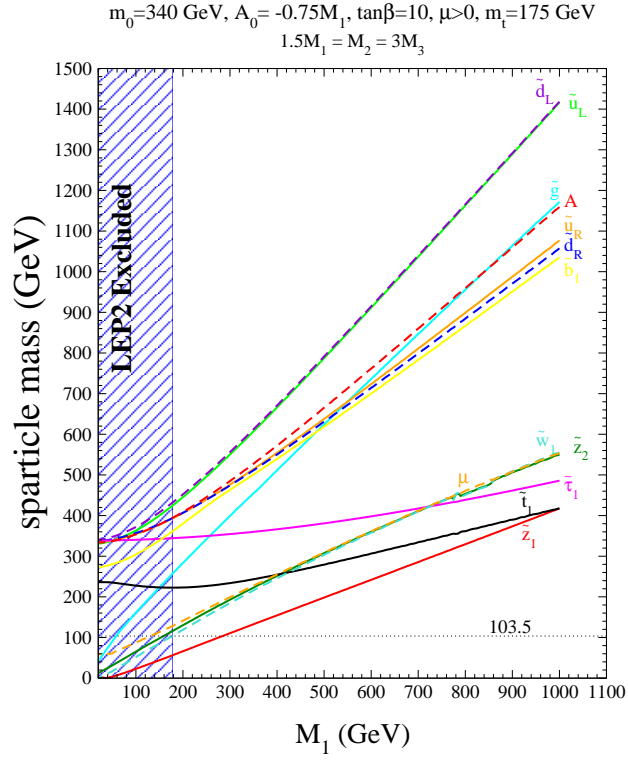


Figure 8: a): Sparticle mass spectrum as a function of the GUT scale gaugino mass M_1 for Case B, where $m_0 = 340$, $1.5M_1 = M_2 = 3M_3$ GeV, $A_0 = -0.75M_1$, $\tan\beta = 10$, $\mu > 0$ and $m_t = 175$ GeV. b): Neutralino relic density versus M_1 for same parameters as in frame a).

$m_0=340$ GeV, $A_0=-0.75M_1$, $\tan\beta=10$, $\mu>0$, $m_t=175$ GeV: $1.5M_1=M_2=3M_3$

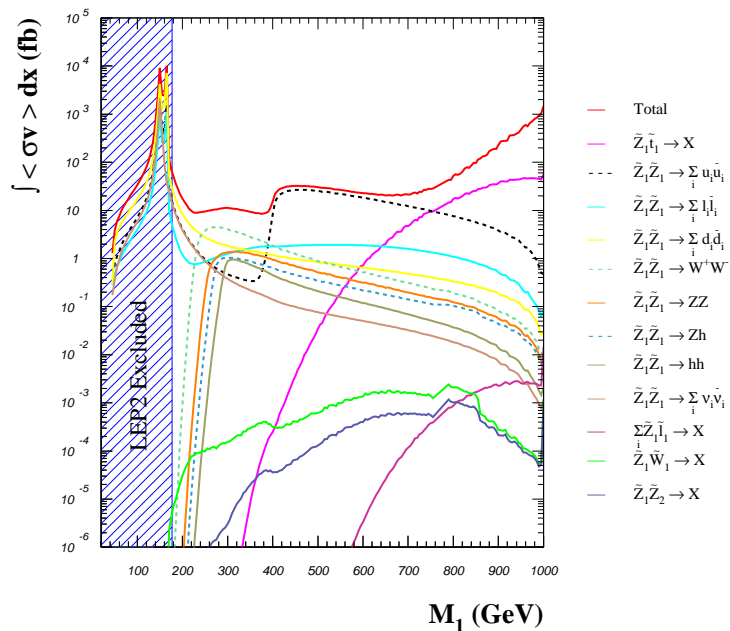


Figure 9: Integrated thermally weighted neutralino annihilation (or co-annihilation) cross sections times relative velocity, for same parameters as in Fig. 8, versus M_1 . The processes shown do not saturate the total at very large values of M_1 because we have not plotted $\tilde{t}_1 \tilde{t}_1$ annihilation which becomes very important there because \tilde{t}_1 becomes very close to $m_{\tilde{Z}_1}$ at the upper end of the M_1 range.

$m_0=340$ GeV, $A_0=-0.75M_1$, $\tan\beta=10$, $\mu>0$, $m_t=175$ GeV
 $1.5M_1 = M_2 = 3M_3$

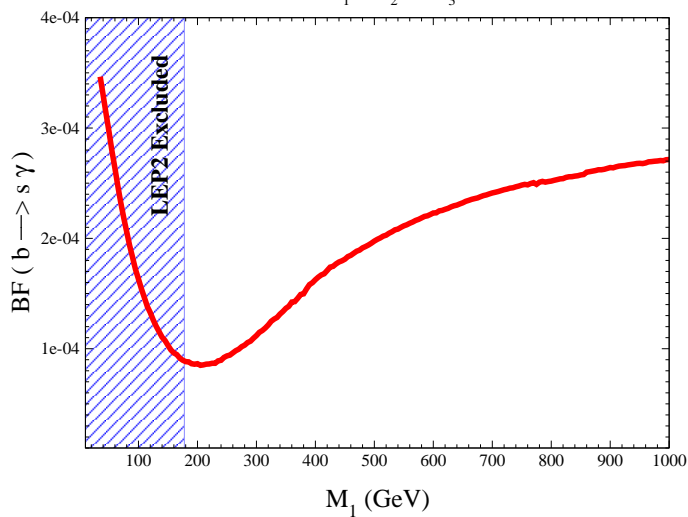


Figure 10: Branching fraction for $b \rightarrow s \gamma$ decay versus M_1 for Case B, for the same model parameters as in Fig. 8.

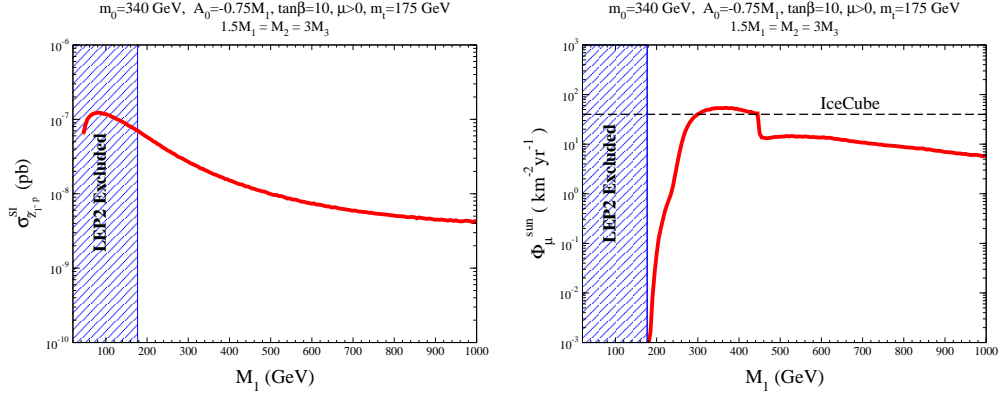


Figure 11: *a)* Spin-independent neutralino-proton scattering cross section and *b)* flux of muons with $E_\mu > 50$ GeV at IceCube versus M_1 for Case B with the same parameters as in Fig. 8.

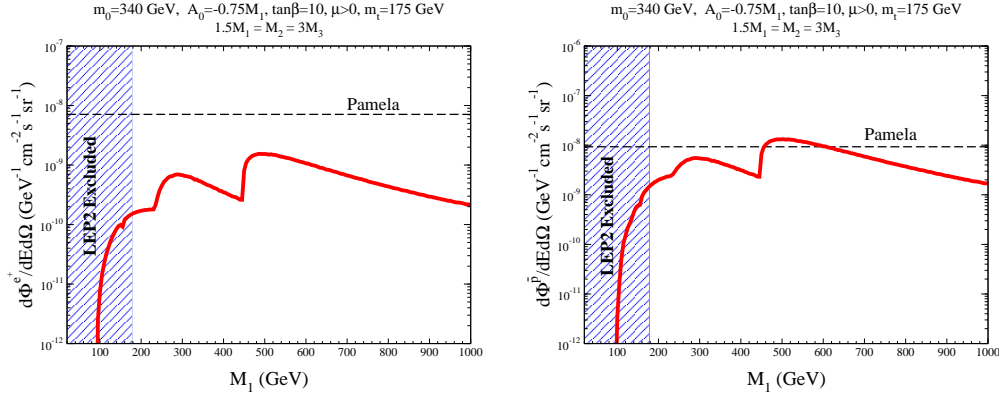


Figure 12: *a)* Expected positron flux and *b)* antiproton flux for Case B versus M_1 for same parameters as in Fig. 8.

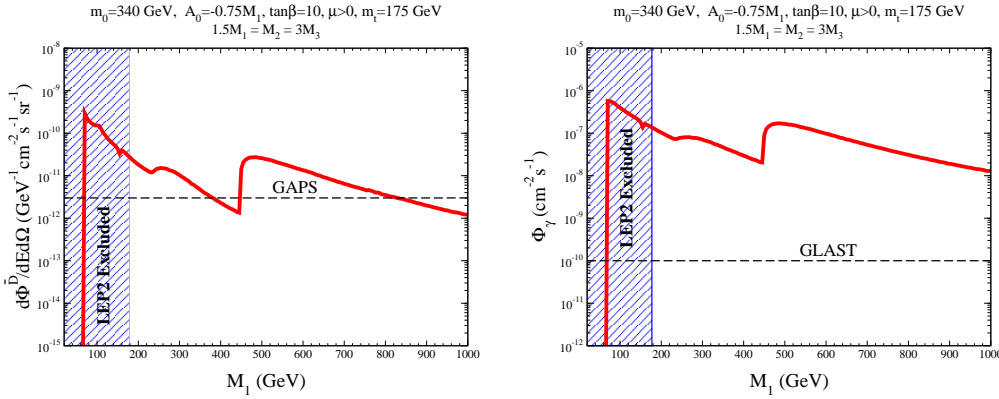


Figure 13: *a)* Expected anti-deuteron flux and *b)* gamma ray flux for the compressed SUSY Case B versus M_1 for same parameters as in Fig. 8.

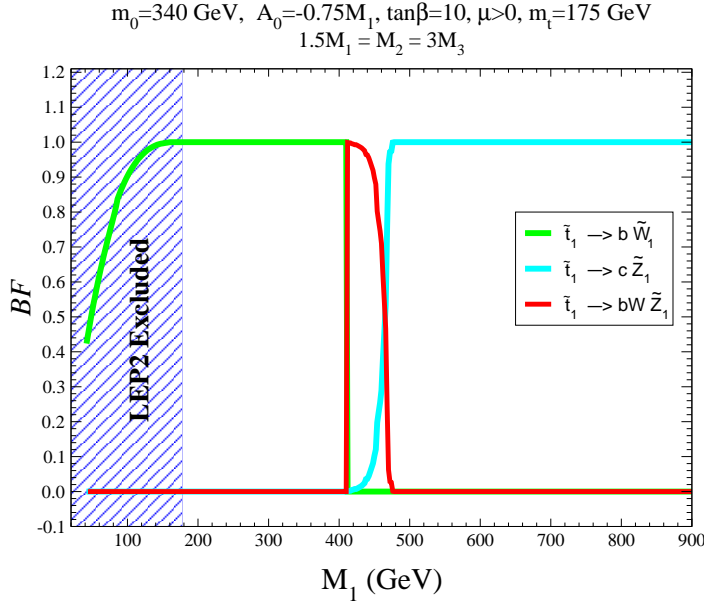


Figure 14: Branching fraction of \tilde{t}_1 vs. GUT scale gaugino mass M_1 for same parameters as in Fig. 8.

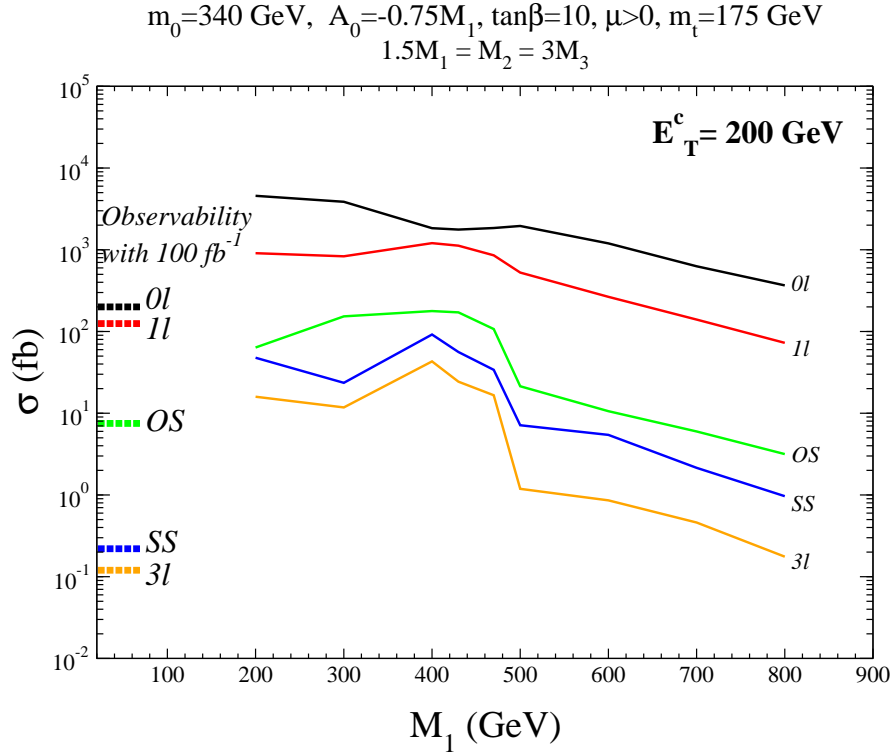


Figure 15: Signal rates for Case B for various multi-jet plus multi-lepton + E_T^{miss} events at the CERN LHC, after cuts detailed in the text and $E_T^c = 200 \text{ GeV}$, versus M_1 for same parameters as in Fig. 8. The horizontal dotted lines show the minimum observable cross section for $E_T^c = 200 \text{ GeV}$, assuming an integrated luminosity of 100 fb^{-1} .